Model-independent extraction of dynamical information from powder diffraction data

Andrew L. Goodwin,[1] Matthew G. Tucker,[1,*] Elizabeth R. Cope,[1] Martin T. Dove,[1,†] and David A. Keen[2,3]
[1]*Department of Earth Sciences, Cambridge University, Downing Street, Cambridge CB2 3EQ, United Kingdom*
[2]*Department of Physics, Oxford University, Clarendon Laboratory, Parks Road, Oxford OX1 3PU, United Kingdom*
[3]*ISIS Facility, Rutherford Appleton Laboratory, Chilton, Didcot, Oxfordshire OX11 0QX, United Kingdom*
(Received 8 February 2005; revised manuscript received 25 August 2005; published 21 December 2005)

We describe a model-independent evaluation of the possibility of extracting detailed lattice dynamical information from neutron powder diffraction data. The method, which we first reported recently [Phys. Rev. Lett. **93**, 075502 (2004)], is extended to include consideration of crystal symmetry. This is exploited to reduce errors in the approach and to allow unambiguous assignment of normal modes. The experimental and computational requirements are explored, with particular attention to the use of the reverse Monte Carlo method for generating atomistic configurations. Phonon-dispersion curves, extracted from neutron total scattering data using the technique, are presented for magnesium oxide and strontium titanate. These are used to illustrate the sensitivity and limitations of this method.

DOI: 10.1103/PhysRevB.72.214304 PACS number(s): 63.20.−e, 61.12.Bt, 02.70.Uu

I. INTRODUCTION

The possibility that neutron powder diffraction (NPD) data might be used to measure phonon-dispersion curves is appealing and has generated recent interest in developing methods of extracting dynamical information from such data.[1–4] The appeal lies in the relative ease with which NPD experiments can be performed; unlike the established experimental techniques of inelastic neutron scattering (INS) and inelastic x-ray scattering (IXS),[5,6] they do not require single-crystal samples and are (by comparison) versatile, time-efficient, and inexpensive.

In principle, the observed scattering function $S(Q)$ contains lattice dynamical information, but the quality of this information is degraded through the integration over dynamical and directional degrees of freedom performed in powder diffraction experiments. There have been a number of recent attempts to quantify the extent to which dynamical information is preserved in this procedure; in general, they have focused upon analysis of the pair distribution function (PDF), which can be derived by Fourier transform of $S(Q)$.[2–4,7]

One proposed approach has involved using the PDF to refine various parameters within standard dynamical models.[2] The expected PDF is calculated from the model, and compared with that from the experimental (NPD) data. An iterative technique, such as the Monte Carlo algorithm, is then used to adjust the input parameters, and the procedure is repeated until a satisfactory fit to data is obtained. For some very simple systems—such as fcc Ni, fcc Ag, and bcc Fe—this method has been shown to give data-driven phonon-dispersion curves that agree with those determined independently from INS experiments to within a few percent accuracy.[4] Materials requiring more complex dynamical models have proved to be a stumbling block for this approach. Moreover, the potential models used in the process have generally been determined (albeit independently) by fitting to INS phonon-dispersion data. The choice of model for any given material may be nontrivial and has been shown to influence strongly the results obtained.[3]

We have recently described a method of probing the dynamical information held within the PDF (and similar diffraction-derived data) directly.[1,8] The technique involves statistical analysis of atomic displacements within large ensembles of atomistic configurations, generated using a data-driven process such as the reverse Monte Carlo (RMC) method. The method differs from those reported previously in that it does not constrain its results in terms of some form of imposed phonon model. This model independence is particularly important when studying systems for which INS/IXS studies are impractical (due to the unavailability of sufficiently large single crystals, for example), where a suitable model may not be known. We hoped that, in the absence of any imposed phonon model, we might be able to determine a more accurate initial indication of the true limitations of NPD as a means of obtaining dynamical information. Indeed, we found that the dynamical information retained within the PDF appeared similar in many ways to that observed using techniques such as INS and IXS; in particular, the low-frequency features appeared to be well-preserved. On the other hand, the PDF appeared insensitive to some details of the dispersion at higher frequencies, such as the LO/TO splitting at the zone center for MgO.

In this sense, the spirit of our present investigation is not so much to evaluate the relative merits of the dynamics-from-diffraction and INS/IXS approaches, but to explore the extent to which dynamical information might be preserved within diffraction data, given that this might be the only practical method for exploring dynamical behavior within many materials. We begin by critically reviewing previous approaches, and continue by establishing the general method by which dynamical information can be accessed from atomistic configurations. We discuss our procedure for generating configurations, and explicitly show its independence from the existence of dynamical information within its output. Our results from applying this method to MgO and $SrTiO_3$, two systems whose lattice dynamics are well understood, are presented and used to assess the relative capabilities and limitations of the approach. We perform additional model calculations to show the extent to which high-

frequency modes contribute to the widths of peaks in the pair distribution function. We complete this paper with a discussion on the prospect for determining dynamical information from powder diffraction data. In some regards we are encouraged that it appears possible to obtain information about the lower-frequency ranges of the phonon-dispersion curves, but we will note that improvements in data collection methods and data analysis will be required to improve the accuracy of the information.

II. DYNAMICS FROM DIFFRACTION: RECENT WORK

The PDF contains information on two-body correlation functions. The connection between these correlation functions and dynamical behavior was realized as early as the 1960s: Kaplow used PDF peak widths to determine empirical vibrational coupling constants for some simple metals at temperatures close to their melting points.[9,10] With the advent of modern synchrotron x-ray and spallation neutron sources, and the contemporaneous increase in accessible computational power, the problem has been revisited several times since the late 1990s.

The recent approaches have developed from the work of Chung and Thorpe, who proposed a formal relationship between the phonons and peak widths in the PDF.[11] They showed that the peak width σ_{ij} corresponding to the pair of atoms (i,j) is given by

$$\sigma_{ij}^2 = \frac{2\hbar}{N}\sum_{\mathbf{k},\nu}\frac{n(\mathbf{k},\nu)+\frac{1}{2}}{\omega(\mathbf{k},\nu)}\left[\frac{1}{2}\left(\frac{|\mathbf{e}(i,\mathbf{k},\nu)\cdot\hat{\mathbf{r}}_{ij}|^2}{m_i}+\frac{|\mathbf{e}(j,\mathbf{k},\nu)\cdot\hat{\mathbf{r}}_{ij}|^2}{m_j}\right)\right.$$
$$\left.-\frac{1}{\sqrt{m_i m_j}}|\mathbf{e}(i,\mathbf{k},\nu)\cdot\hat{\mathbf{r}}_{ij}||\mathbf{e}(j,\mathbf{k},\nu)\cdot\hat{\mathbf{r}}_{ij}|\exp(i\mathbf{k}\cdot\hat{\mathbf{r}}_{ij})\right], \quad (1)$$

where the sum is over all modes ν and wave vectors $\mathbf{k}$. The $\mathbf{e}(i,\mathbf{k},\nu)$ are the mass-weighted normalized mode displacement vectors, $n(\mathbf{k},\nu)$ and $\omega(\mathbf{k},\nu)$ are the mode occupation number and mode (angular) frequency, respectively, N is the number of unit cells, m_i is the atomic mass, and $\hat{\mathbf{r}}_{ij}$ is the unit vector directed from the equilibrium position of atom i to that of atom j. They applied this theory to a series of semiconductor alloys. The excellent agreement obtained between calculated and experimental PDF showed that the form of the PDF could indeed be accounted for in terms of a reasonable potential model.

Predicting diffraction data from a dynamical model is a fundamentally different task from predicting a dynamical model from diffraction data. The problem is that Eq. (1) is not invertible: one cannot express (at least starting from this relationship) the mode frequencies and displacement vectors in terms of the observed peak widths.

Subsequently, Dimitrov and co-workers suggested that, if one can calculate a PDF from a dynamical model, then one should be able to use the fit between calculated and observed PDFs to refine the model parameters.[2] In doing so, one would obtain a potential model whose parameters were driven wholly by the available data. The authors presented results for two systems—Ni and CaF_2—chosen as they required rather different interatomic potentials to describe their lattice dynamics. Both systems gave phonon-dispersion curves that were essentially indistinguishable from those obtained from INS experiments.

The usefulness of this approach has been disputed by Reichardt and Pintschovius, who showed that different potential models could give rise to essentially identical PDFs.[3] However, the different models gave similar phonon-dispersion curves, which is why the different models gave similar PDFs. Thus it could be argued that what was really demonstrated was that different models can give rise to similar dispersion curves. Nonetheless, the report raised serious questions about the possibility of extracting phonons from diffraction data.

More recently, Graf and co-workers readdressed the problem from an alternative viewpoint.[4] Their approach was to take a basic phonon model, in which the number of parameters could be systematically varied. For a given system, a set of "reference" parameters was assigned, and this was used to generate a synthetic PDF together with the corresponding synthetic phonon-dispersion curves. Starting from just one parameter, and progressing toward the full complement (i.e., as many as were used to generate the synthetic data sets), the values of the parameters themselves were refined according to the method of Dimitrov *et al.*[2] Upon convergence, the set of phonon-dispersion curves given by the refined parameters was calculated, and compared to that obtained from the synthetic set. Goodness-of-fit values $\chi_{\mathrm{pdf}}, \chi_{\mathrm{phonon}}$ could be determined for both the PDFs and the dispersion curves.

The authors observed different behavior for different materials, distinguished primarily by the complexity of their lattice dynamics. For "simple" systems, such as bcc Fe, the parameters converged on those used to generate the original synthetic data set; moreover, as the number of parameters was increased, both χ_{pdf} and χ_{phonon} decreased monotonically. On the other hand, "complex" materials—a term that included bcc Nb—behaved rather differently. Even when all parameters were allowed to vary, the system did not converge on the same set of parameters as those used to generate the synthetic data sets. Additionally, in some instances, an increase in the number of force constants refined resulted in an improved value of χ_{pdf} but an increase in χ_{phonon} (or vice versa). The authors interpreted these results as an indication that one could not use diffraction data to determine phonon-dispersion curves for materials with "complex" dynamics. Since the distinction between "simple" and "complex" is one that can only be applied *a posteriori*, they suggested that the method was unlikely to be of any general use.

In retrospect, some aspects of this most recent report give cause for concern, and one especially so. In the instance in which the number of parameters included in the refinement process was equal to the number used to generate the synthetic data sets, there must—without question—exist a solution for which $\chi_{\mathrm{pdf}}=0$ and $\chi_{\mathrm{phonon}}=0$ (the latter would not affect the fitting procedure, of course): it is given by the very parameters used to generate the synthetic data sets themselves. That this solution was not found for a number of systems would indicate that the refinement procedure used by the authors did not arrive at the global minimum in these instances, and raises the possibility that the same was true

when fewer parameters were included in the refinement process. This immediately casts suspicion on any inference drawn from the relative behavior of χ_{pdf} and χ_{phonon} in that study, especially for "complex" systems.

What is clear from this body of work is that reasonable phonon models give reasonable fits to the PDF data. Also, if different models produce similar dispersion curves, they will give similar fits to the PDF. What is needed is an approach that does not rely on the use of particular phonon models. In other words, is it possible to extract dynamical information from diffraction data as mode frequencies and displacement vectors, rather than as parameters in a predetermined interaction potential? This is the key question we aim to address in this paper.

III. THEORY

A. Extraction of dynamical quantities from atomistic configurations

Traditionally, the atomic-scale structures of crystalline materials are reduced to the average atomic positions within the crystallographic unit cell. Some additional information in terms of the atomic dynamics is given in the displacement parameters of each atom, which correspond to its root-mean-squared displacement from the average position. With the advent of diffractometers capable of measuring simultaneously the intensities of Bragg reflections and diffuse scattering (such as the GEM instrument at ISIS[12,13]), it has become increasingly possible to resolve short-range structural features in the same materials.

One method of visualizing these features is through refinement of atomistic configurations consistent with diffraction data. These configurations essentially represent a crystallographic supercell, with no implicit symmetry constraints on the atomic positions. The average structure across the configuration matches that obtained through traditional refinement methods—such as the Rietveld method—and so both store the same long-range structural information. However, the short-range information can be incorporated within the configuration in the form of individual atomic displacements.

To a first approximation, these displacements are determined by the nature of the phonon modes that govern the lattice dynamics of the material. Indeed, the configuration can be considered as a "snapshot" of the atoms undergoing vibrational motion. Consequently, the configurations are far from unique; different configurations can essentially be considered as "snapshots" of the same set of atoms taken at different times and as such are equally consistent with the experimental diffraction data.

There is a rigorous link between the nature of the phonon modes and the displacements we might observe in an atomistic configuration.[14,15] For each atom j in the unit cell ℓ, the instantaneous displacement $\mathbf{u}(j\ell,t)$ from its equilibrium position $\mathbf{r}(j\ell)$ is given by the linear superposition of the effects of all phonon modes ν at all wave vectors $\mathbf{k}$,

$$\mathbf{u}(j\ell,t)=\sum_{\mathbf{k},\nu}\hat{\mathbf{u}}(j,\mathbf{k},\nu)\exp\{\mathrm{i}[\mathbf{k}\cdot\mathbf{r}(j\ell)-\omega(\mathbf{k},\nu)t]\}. \quad (2)$$

Here, $\hat{\mathbf{u}}(j,\mathbf{k},\nu)$ is the amplitude vector of the mode ν at wave vector $\mathbf{k}$. This quantity may be decomposed further,

$$\hat{\mathbf{u}}(j,\mathbf{k},\nu)=\frac{\hat{u}(\mathbf{k},\nu)}{\sqrt{Nm_j}}\mathbf{e}(j,\mathbf{k},\nu), \quad (3)$$

where $\mathbf{e}(j,\mathbf{k},\nu)$, N, and m_j retain their meanings from Eq. (1). The scalar quantity $\hat{u}(\mathbf{k},\nu)$ is the normalized mode amplitude, and is independent of the type of atom j. The sets of vectors $\mathbf{e}(j,\mathbf{k},\nu)$ corresponding to any two modes ν,ν' are orthonormal,

$$\sum_j \mathbf{e}(j,\mathbf{k},\nu)\cdot\mathbf{e}(j,-\mathbf{k},\nu')=\delta(\nu,\nu'). \quad (4)$$

Being parallel to the $\hat{\mathbf{u}}(j,\mathbf{k},\nu)$, they describe the characteristic relative atomic motions associated with the mode.

It is convenient to subsume both the normalized mode amplitude and the time dependence into the normal mode coordinate $Q(\mathbf{k},\nu,t)$,

$$Q(\mathbf{k},\nu,t)=\hat{u}(\mathbf{k},\nu)\exp[-\mathrm{i}\omega(\mathbf{k},\nu)t], \quad (5)$$

which, upon substitution into Eq. (2), gives

$$\mathbf{u}(j\ell,t)=\frac{1}{\sqrt{Nm_j}}\sum_{\mathbf{k},\nu}\mathbf{e}(j,\mathbf{k},\nu)\exp[\mathrm{i}\mathbf{k}\cdot\mathbf{r}(j\ell)]Q(\mathbf{k},\nu,t). \quad (6)$$

The normal mode coordinates are useful quantities as their time averages are related directly to the normal mode frequencies,[15]

$$\langle|Q(\mathbf{k},\nu)|^2\rangle=\frac{\hbar}{\omega(\mathbf{k},\nu)}\left[n(\mathbf{k},\nu)+\frac{1}{2}\right]. \quad (7)$$

In the high-temperature limit ($k_{\mathrm{B}}T\gg\hbar\omega$), Eq. (7) has the simpler form

$$\langle|Q(\mathbf{k},\nu)|^2\rangle=\frac{k_{\mathrm{B}}T}{\omega^2(\mathbf{k},\nu)}. \quad (8)$$

These quantities can also be expressed in terms of the instantaneous atomic displacements $\mathbf{u}(j\ell,t)$ by reverse Fourier transform of Eq. (6),

$$Q(\mathbf{k},\nu,t)=\frac{1}{\sqrt{N}}\sum_{j,\ell}\sqrt{m_j}\exp[\mathrm{i}\mathbf{k}\cdot\mathbf{r}(j\ell)]\mathbf{e}^*(j,\mathbf{k},\nu)\cdot\mathbf{u}(j\ell,t). \quad (9)$$

It is this connection between the atomic displacements and the normal mode frequencies, via the $Q(\mathbf{k},\nu,t)$, that underpins our approach to extracting phonons from atomistic configurations. Equation (9) essentially describes a change of basis between these two quantities, with the mapping given by the mode displacement vectors $\mathbf{e}^*(j,\mathbf{k},\nu)$. We can extend this concept mathematically by assembling the $Q(\mathbf{k},\nu,t)$ for all modes ν into a single column vector $\mathbf{Q}(\mathbf{k},t)$. There will be $3Z$ components to this vector, where Z is the number of atoms in the (primitive) unit cell. The corresponding set of Eqs. (9) is given by the relation

$$\mathbf{Q}(\mathbf{k},t)=\mathbf{A}(\mathbf{k})\cdot\mathbf{T}(\mathbf{k},t). \quad (10)$$

Here, $\mathbf{A}(\mathbf{k})$ is a $3Z\times3Z$ matrix whose rows index the $3Z$ normal modes ν and the columns the displacements of each atom j along the Cartesian axes $\alpha\in\{x,y,z\}$. Its entries

$A_{\nu,\alpha j}(\mathbf{k})$ are given by the Cartesian components $e^*_\alpha(j,\mathbf{k},\nu)$ of the mode displacement vectors. The column vector $\mathbf{T}(\mathbf{k},t)$ is defined by the atomic displacements $u_\alpha(j\ell,t)$ along the Cartesian axes,

$$T_{\alpha j}(\mathbf{k},t) = \sqrt{\frac{m_j}{N}} \sum_\ell u_\alpha(j\ell,t)\exp[\mathrm{i}\mathbf{k}\cdot\mathbf{r}(j\ell)]. \tag{11}$$

Importantly, the elements of $\mathbf{T}(\mathbf{k},t)$ are quantities we are able to calculate directly from our atomistic configurations. In principle, Eq. (10) could be used to convert these values to the elements of $\mathbf{Q}(\mathbf{k},t)$; however, this would require explicit knowledge of the normal displacement vectors. Rather, our understanding of these vectors is limited to their orthonormality, a property we proceed to exploit.

First, the time-averaged matrix $\mathbf{S}(\mathbf{k})$ is calculated using the relation

$$\mathbf{S}(\mathbf{k}) = \langle \mathbf{T}(\mathbf{k}) \cdot \mathbf{T}^{\mathrm{T}}(-\mathbf{k}) \rangle. \tag{12}$$

In the present context, the concept of "time-averaging" corresponds to taking averages over large numbers of configurations. The error associated with this assumption scales inversely with the square root of the number of configurations. The usefulness of the quantity $\mathbf{S}(\mathbf{k})$ lies in the property that the basis of $\mathbf{Q}(\mathbf{k},t)$ is the set of normal coordinates and hence the matrix $\mathbf{\Omega}(\mathbf{k}) = \langle \mathbf{Q}(\mathbf{k}) \cdot \mathbf{Q}^{\mathrm{T}}(-\mathbf{k}) \rangle$ is diagonal with entries (in the high-temperature limit)

$$\Omega_{i,i}(\mathbf{k}) = \frac{k_{\mathrm{B}}T}{\omega^2(\mathbf{k},i)}. \tag{13}$$

Substitution of Eq. (10) into Eq. (12) gives

$$\mathbf{\Omega}(\mathbf{k}) = \mathbf{A}(\mathbf{k}) \cdot \mathbf{S}(\mathbf{k}) \cdot \mathbf{A}^{\mathrm{T}}(\mathbf{k}), \tag{14}$$

which essentially represents a matrix diagonalization problem. The uniqueness of diagonalization yields the elements of $\mathbf{\Omega}(\mathbf{k})$ (and hence the mode frequencies) from $\mathbf{S}(\mathbf{k})$. Furthermore, the eigenvectors of $\mathbf{S}(\mathbf{k})$ are the elements of $\mathbf{A}(\mathbf{k})$. In this way, the method yields both the frequencies and normal mode displacement vectors of the phonons at arbitrary wave vector.

B. Symmetry considerations

The choice of basis for $\mathbf{T}(\mathbf{k},t)$ is somewhat arbitrary; atom/Cartesian direction coordinates have been used in the above analysis solely for the purpose of simplicity. However, any basis that spans the same vector space as these will allow calculation of $\mathbf{S}(\mathbf{k})$ and, in turn, the normal mode coordinates and frequencies. It is reasonable then to question whether a more judicious choice of basis might exist than the one suggested above. In addressing this issue, we explore the means by which knowledge of the underlying symmetry of the structure in question can assist in choosing a suitable basis for $\mathbf{T}(\mathbf{k},t)$, simplifying the form of $\mathbf{S}(\mathbf{k})$ and allowing detailed insight into the nature of each normal mode.

The analysis begins by explicating the relationship between $\mathbf{S}(\mathbf{k})$ and the dynamical matrix $\mathbf{D}(\mathbf{k})$. There is an immediate natural connection between these two matrices as, in both cases, their eigenvalues are directly related to the normal mode frequencies. On the one hand, $\mathbf{S}(\mathbf{k})$ stores this information in terms of the mass-weighted displacements of the atoms while $\mathbf{D}(\mathbf{k})$ is constructed from the individual forces between atoms. This can be seen more formally by considering explicitly the elements of each matrix,

$$S_{\alpha j,\beta j'}(\mathbf{k}) = (m_j m_{j'})^{1/2} \sum_{\ell\ell'} \Delta_{\alpha,\beta}\begin{pmatrix} jj' \\ \ell\ell' \end{pmatrix} \times \exp\{\mathrm{i}\mathbf{k}\cdot[\mathbf{r}(j'\ell') - \mathbf{r}(j\ell)]\}, \tag{15}$$

$$D_{\alpha j,\beta j'}(\mathbf{k}) = \frac{1}{(m_j m_{j'})^{1/2}} \sum_{\ell'} \Phi_{\alpha,\beta}\begin{pmatrix} jj' \\ 0\ell' \end{pmatrix} \times \exp\{\mathrm{i}\mathbf{k}\cdot[\mathbf{r}(j'\ell') - \mathbf{r}(j0)]\}. \tag{16}$$

In both instances, the elements correspond to correlations between the pair of atoms j and j' along the axes α and β ($\alpha,\beta \in \{x,y,z\}$), respectively. $\mathbf{\Delta}$ and $\mathbf{\Phi}$ are the displacement and force constant matrices, respectively, whose elements are given by

$$\Delta_{\alpha,\beta}\begin{pmatrix} jj' \\ \ell\ell' \end{pmatrix} = \frac{\langle u_\alpha(j\ell) u_\beta(j'\ell') \rangle}{N}, \tag{17}$$

$$\Phi_{\alpha,\beta}\begin{pmatrix} jj' \\ \ell\ell' \end{pmatrix} = \frac{\partial^2 W}{\partial u_\alpha(j\ell)\partial u_\beta(j'\ell')}, \tag{18}$$

where W is the lattice energy. Finally, Eqs. (15) and (16) give the relation (in the high-temperature limit)

$$\mathbf{S}(\mathbf{k}) \cdot \mathbf{D}(\mathbf{k}) = k_{\mathrm{B}}T. \tag{19}$$

The purpose of establishing this relationship between the normal mode coordinates and the dynamical matrix is that significant effort has previously been expended in finding ways of simplifying the dynamical matrix; by association, we can use these same methods to simplify $\mathbf{S}(\mathbf{k})$.

The essential concept is that $\mathbf{D}(\mathbf{k})$—and hence $\mathbf{S}(\mathbf{k})$—must be left invariant when acted upon by the symmetry operations of the space group of the crystal itself.[16–18] Formally, this can be expressed by the statement

$$\mathbf{S}(\mathbf{k}) = \mathbf{\Theta}(\mathbf{k};i) \cdot \mathbf{S}(\mathbf{k}) \cdot \mathbf{\Theta}(\mathbf{k};i)^{-1}, \quad \forall\, i, \tag{20}$$

where $\mathbf{\Theta}(\mathbf{k};i)$ is a matrix representation of the ith symmetry operation of the space group acting at the wave vector $\mathbf{k}$. These relations place (often severe) restrictions on the values elements of $\mathbf{S}(\mathbf{k})$ can assume. Some might be zero, some the same as other elements, or indeed some the linear combinations of a number of elements in the matrix.

An elegant group theoretical approach has shown that a symmetry-reduced matrix $\hat{\mathbf{H}}(\mathbf{k})$, composed of a minimal number of independent matrix elements, can be constructed by successive matrix transformations of a random Hermitian matrix $\mathbf{H}$ by the $\mathbf{\Theta}(\mathbf{k};i)$,[19]

$$\hat{\mathbf{H}}(\mathbf{k}) = \sum_i \mathbf{\Theta}(\mathbf{k};i) \cdot \mathbf{H} \cdot \mathbf{\Theta}(\mathbf{k};i)^{-1}. \quad (21)$$

Importantly, this simplification allows calculation of a matrix $\mathbf{V}(\mathbf{k})$ that is capable of block-diagonalizing each of the $\mathbf{\Theta}(\mathbf{k};i)$, and hence is also capable of block-diagonalizing $\hat{\mathbf{H}}(\mathbf{k})$.[16] The columns of $\mathbf{V}(\mathbf{k})$ are the symmetry-coordinate vectors, and if we express $\mathbf{S}(\mathbf{k})$ with these as a basis, the resulting matrix $\hat{\mathbf{S}}(\mathbf{k})$ will be in block-diagonal form.

This serves to reduce the diagonalization problem of Eq. (14) to the diagonalization of the set of (smaller) blocks of $\hat{\mathbf{S}}(\mathbf{k})$,

$$\mathbf{\Omega}_i(\mathbf{k}) = \hat{\mathbf{A}}_i(\mathbf{k}) \cdot \hat{\mathbf{S}}_i(\mathbf{k}) \cdot \hat{\mathbf{A}}_i^{\mathrm{T}}(\mathbf{k}), \quad (22)$$

where i runs over all blocks in $\hat{\mathbf{S}}(\mathbf{k})$. Each block in this matrix now corresponds to a single type of symmetry; in the appropriate group theoretical language, the blocks can be associated with irreducible representations (IRs) of the point group of the wave vector.[17] It is possible that more than one mode will correspond to a given IR and that some IRs may not correspond to any modes at all. Nevertheless, the modes from different blocks are precluded from mixing and so their individual contributions to $\mathbf{S}(\mathbf{k})$ can be separated. The eigenvectors $\hat{\mathbf{A}}_i(\mathbf{k})$ are expressed in the basis of symmetry-coordinate vectors, and so must be converted back to atom-direction coordinates to correspond to the related entries of $\mathbf{A}(\mathbf{k})$. Importantly, they now give the symmetry-adapted mode displacement vectors.

In practice, those elements of $\hat{\mathbf{S}}(\mathbf{k})$ that do not belong to one of these blocks [i.e., the off-(block)-diagonal entries] tend to have small, but nonzero, values. This is a product of the implicit errors associated with the construction of $\mathbf{S}(\mathbf{k})$ from the average of a finite set of configurations and errors introduced during the generation of the atomistic configurations. The exclusion of these values from the matrix diagonalization procedure serves to reduce the associated error in the mode frequencies obtained.

We have shown how the diagonalization process might be simplified through the appropriate choice of a symmetry-adapted basis. The group theoretical analysis required to calculate this basis is formidable and it is fortunate that excellent reviews for such a treatment of the dynamical matrix exist in the literature.[16,17,19] The method is valuable in that it both reduces the computational effort of the diagonalization procedure represented by Eq. (14) and provides a means by which both the symmetry and the mode displacement vectors of all normal modes may be assigned without ambiguity.

IV. GENERATION OF ATOMISTIC CONFIGURATIONS

A. Reverse Monte Carlo method

We were encouraged by a recent study in which the relevant analysis of reverse Monte Carlo configurations of α- and β-quartz, generated by fitting to NPD data, was able to reproduce detailed single-crystal diffuse scattering patterns.[20] Such patterns are direct manifestations of the phonon energies and dispersion, and their preservation within RMC configurations suggests the method is an appropriate tool with which to probe the extent of dynamical information accessible from NPD data.

The RMC procedure, discussed in detail elsewhere,[21,22] involves minimization of the "mismatch" function

$$\chi^2_{\mathrm{RMC}} = \chi^2_{S(Q)} + \chi^2_{T(r)} + \chi^2_{\mathrm{Bragg}}, \quad (23)$$

where

$$\chi^2_{S(Q)} = \sum_k \sum_j [S_{\mathrm{calc}}(Q_j)_k - S_{\mathrm{exp}}(Q_j)_k]^2/\sigma_k^2(Q_j),$$

$$\chi^2_{T(r)} = \sum_j [T_{\mathrm{calc}}(r_j) - T_{\mathrm{exp}}(r_j)]^2/\sigma^2(r_j),$$

$$\chi^2_{\mathrm{Bragg}} = \sum_{hkl} [I_{\mathrm{calc}}(hkl) - I_{\mathrm{exp}}(hkl)]^2/\sigma^2(hkl). \quad (24)$$

Here, the $\chi^2_{S(Q)}$ contribution includes components from each of k data sets. The radial distribution function $T(r)$, chosen for convenience, is related to the partial pair distribution functions $g_{ij}(r)$ and is given by

$$T(r) = 4\pi r \rho_0 \left\{ \sum_{ij} c_i c_j \bar{b}_i \bar{b}_j [g_{ij}(r) - 1] + \left(\sum_i c_i \bar{b}_i \right)^2 \right\}, \quad (25)$$

where ρ_0 is the configuration number density, c_i is the concentration of species i, and $\bar{b}_i$ is its neutron scattering length.[23] There are various forms similar to the functions $S(Q)$ and $T(r)$ that may be used with equivalent results. The use of both real-space and reciprocal-space terms is important, as each accentuates different structural features. For this same reason, we include consideration of the Bragg scattering intensities, which ensure our configurations are consistent with the Rietveld-refined average crystal structure; moreover, they add some additional dimensionality to the process through assignment of the Miller indices. In this way, the data constrain both the single-atom (Bragg) and pair (PDF) correlation functions of the configurations.

In its minimization procedure, the RMC method generates random atomic moves, calculating at each stage the concomitant effect $\Delta\chi^2$ on the overall mismatch function. Any move for which $\Delta\chi^2 < 0$ is accepted automatically, while others are accepted only with probability $\exp(-\Delta\chi^2/2)$. The algorithm is repeated until χ^2 has converged to some equilibrium value. At this point, the RMC fit to the experimental data will be to within the errors σ_j. It is possible to continue running the RMC algorithm on these equilibrium configurations; while the fits to data do not improve further, the method continues to generate and accept moves, such that configurations separated by sufficiently many moves may be considered independent. When generating ensembles of configurations for our phonon analysis, we used equilibrium configurations separated by at least $N \ln 10$ atom moves: one can expect at least 90% of atoms to have moved under these conditions.

The fitting procedure itself is performed by the suite of

programs RMCPROFILE.[21,24] Final output from the procedure is in the form of the atomistic configurations themselves, with each configuration capable of reproducing the observed structural data to within the specified error limits. In this sense, the RMC method is more similar to a refinement process than a modeling tool; its output is driven wholly by experimental data. The most obvious difference between the RMC approach and a typical least-squares refinement is the possibility that unfavorable moves might be accepted during the refinement procedure. Its effect is to maximize the amount of configuration space that RMC is able to sample. In principle, it ensures the method finds the global energy minimum, given a sufficient number of iterations.

There are two "popular" concerns frequently expressed about the RMC procedure: first, the equilibrium configurations obtained are rarely unique, and second, the technique favors high-entropy configurations (as they are more likely to be sampled). The uniqueness problem is not surprising given the large number of variables refined in each configuration, and means that care must be taken in choosing which conclusions might be justifiably drawn from an individual RMC configuration. We have already mentioned that one way of interpreting this degeneracy is in terms of different solutions corresponding to snapshots of the same set of atoms at different times; that is, one can view equivalent (yet different) configurations as different superpositions of the normal modes on the same set of atoms. Indeed, it is this very degeneracy that we require when extracting dynamical information from ensembles of configurations.

The prevalence of high-entropy configurations is potentially problematic in that we cannot be certain that such configurations represent the most realistic picture of the local atomic displacements in a given material. The consideration of Bragg intensities within the refinement procedure serves to reduce its effects somewhat; however, configurations generated using this basic RMC method routinely contain regions whose local structure is highly distorted, with chemically unreasonable atomic positions [Fig. 1(a)]. The incorporation of spurious atomic displacements within configurations has significant ramifications for any proposed extraction of dynamical information, giving rise to (often severe) anisotropy and a concomitant reduction in the quality of any results obtained.

B. Atomistic restraints and constraints

One method of addressing the entropy problem is to introduce a number of constraints and restraints on the fitting procedure. In all cases, the underlying principle is to use sound chemical and physical knowledge to prevent RMC arriving at chemically or physically unreasonable configurations. Perhaps the simplest constraint—the "closest-approach" constraint—prohibits atoms from approaching each other closer than some physically sensible distance [typically chosen to coincide with the start of the first observed peak in the experimental $T(r)$ function]. For some systems with very simple structures, implementation of this constraint within the RMC algorithm can be sufficient to temper the incorporation of damaged regions within configurations; in general, however, this is not the case.

1. Bond length and bond angle restraints

An additional restraint, in which individual bond lengths and bond angles are prevented from drifting from their known values, has been proposed[25,26] and has been successful in moderating disorder in a number of systems [Fig. 1(b)].[27,28] It involves the incorporation of additional energy terms in the calculation of χ^2 of the form

$$\chi^2_{\text{bond}} = \sum_{\text{bonds}} |r - \bar{r}|^2/\sigma^2_{\text{bonds}},$$

$$\chi^2_{\text{angle}} = \sum_{\text{angles}} |\theta - \bar{\theta}|^2/\sigma^2_{\text{angles}}. \tag{26}$$

Here, $\bar{r}$ and $\bar{\theta}$ are mean bond lengths and bond angles, respectively, and σ_{bonds}, σ_{angles} their standard deviations. These values can be obtained from the experimental radial distribution function.[29] Such restraints serve to restrict the set of configurations generated by RMC to those that contain physically reasonable bond lengths and bond angles [for which the contribution of the terms represented by Eq. (26) to the value of χ^2_{RMC} is minimal].

The RMC method, moderated using the constraints and restraints detailed above, has historically been used to generate realistic atomistic configurations, from which some conclusions about static short-range and long-range structural features can be drawn. For these purposes, the method appears to work well as it stands. However, in our attempt to extract dynamical information from these configurations, we are asking very different and subtle questions of the data. Consequently, it is essential that we ensure that any additional constraints used in the refinement procedure do not prejudice the dynamical information retrievable from the resulting configurations.

In this context, we note that the bond length/bond angle restraints act as harmonic potential functions, modeling interatomic bonds and three-body angles as harmonic oscillators, with the force constants entering in the form of the σ_{bonds} and σ_{angles} values. To test whether the implementation of these restraints has any effect on the phonon-dispersion curves obtained, we used the RMC procedure to generate two different configurational ensembles each corresponding to a $15\times15\times15$ supercell of $SrTiO_3$. In order to control against the influence of diffraction data itself on the phonon dispersion, no actual data sets were used to constrain the fits in either instance. The ensembles differed in that the first was allowed to proceed without any potential restraint; as such, the atoms in these configurations—constrained neither by data nor by imposed restraints—essentially followed a "random walk" about their initial positions. On the other hand, a potential restraint was applied to the second ensemble, using typical values of σ_{bonds} and σ_{angles}.

In each case, 300 configurations were generated, and the corresponding phonon-dispersion curves calculated along high-symmetry directions. Our results [Figs. 2(a) and 2(b)] clearly indicate that the inclusion of potential restraints

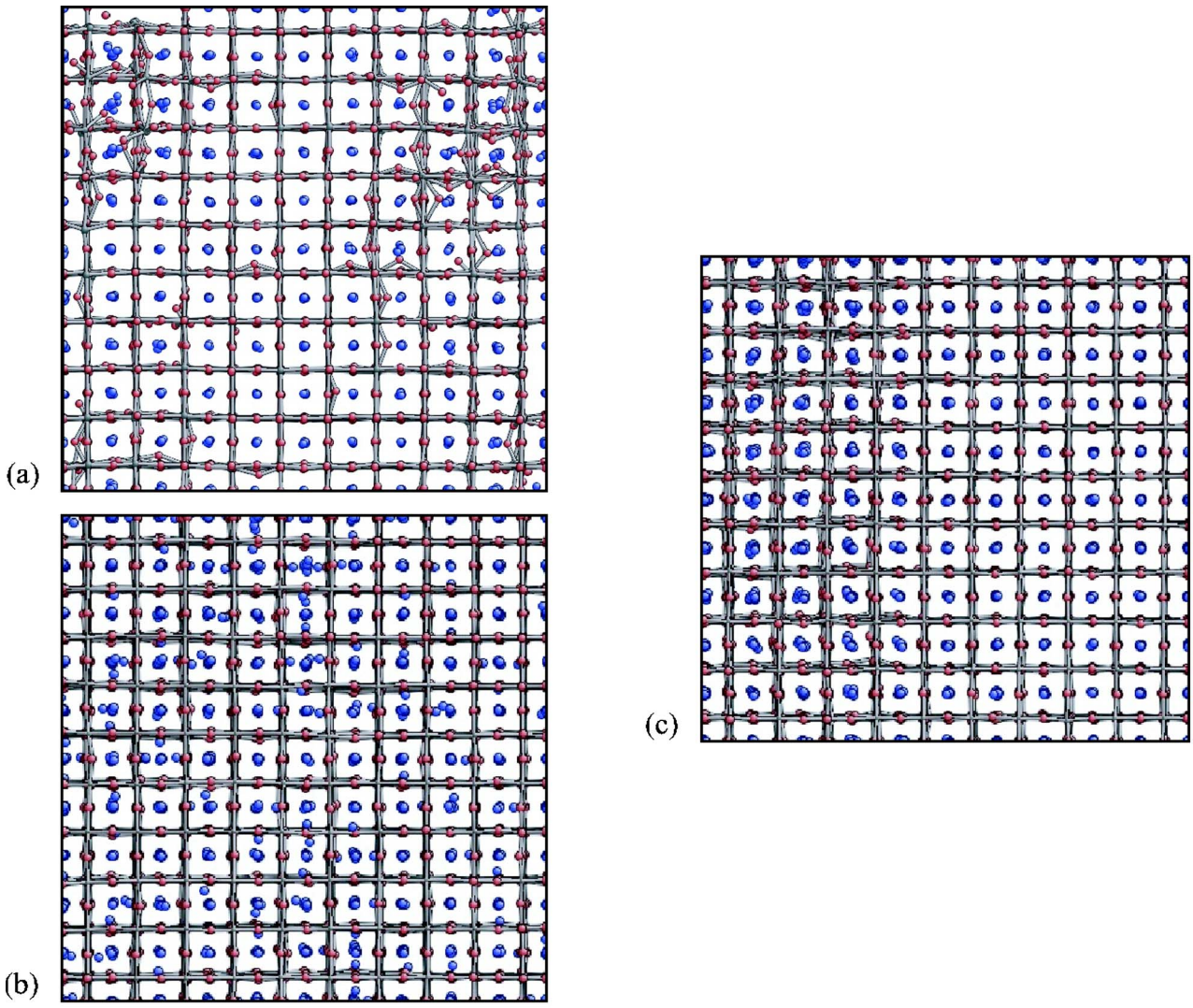

FIG. 1. (Color online) Regions of equilibrium RMC configurations representing a $10\times10\times10$ supercell of $SrTiO_3$ generated from NPD data at 295 K. (a) In the absence of any constraints or restraints, RMC introduces a number of regions of localized "damage," which involve unreasonable bond distances and bond angles. (b) The use of Ti–O bond length and O–Ti–O bond angle restraints successfully moderates the behavior of the Ti/O framework, but the displacement of the unrestrained Sr atoms (shown here as unbonded atoms) increases to an unrealistic level in response. (c) Implementation of the DW constraint avoids the introduction of damaged regions, and allows small concerted displacements of large regions of the configurations (corresponding to large wavelength acoustic modes). All three configurations give essentially identical fits to data.

within the RMC procedure has a pronounced effect on the shape of the phonon-dispersion curves. As expected, those curves generated from the potential-free configurations show negligible dispersion across the Brillouin zone (BZ), while many features—including mode softening near the zone center and zone boundary—are distinguishable within those generated using the potential restraint. We would emphasize here that the phonon-dispersion curves shown in Fig. 2 were calculated from RMC configurations that had never seen diffraction data. The RMC procedure was driven only by constraints (if present), and consequently the presence of large error bars is not surprising. For those curves determined without any constraints [Fig. 2(a)], there are no regions of the phonon spectrum—between approximately 3 and 20 THz—that are not within one standard deviation of some mode. On the other hand, there are a number of such regions in the curves determined using the bond-angle constraints described above [Fig. 2(b)]—in spite of the absence of any diffraction data to drive the dispersion.

This effect is easily rationalized in terms of those sets of atomic motions that have no effect on χ^2_{bond} and χ^2_{angle}. Such moves are inherently more likely to be accepted, and their concomitant predominance among the configurations will be reflected in a low value of the associated mode frequency. For $SrTiO_3$, there are two types of motion that fall into this category: translations of the Sr atoms (which are left untethered by the potential constraints) and "rigid-unit"-type displacements, which correspond to the octahedral tilting mode. Indeed, inspection of the associated normal displacement vectors reveals the effect of both types of motion on the

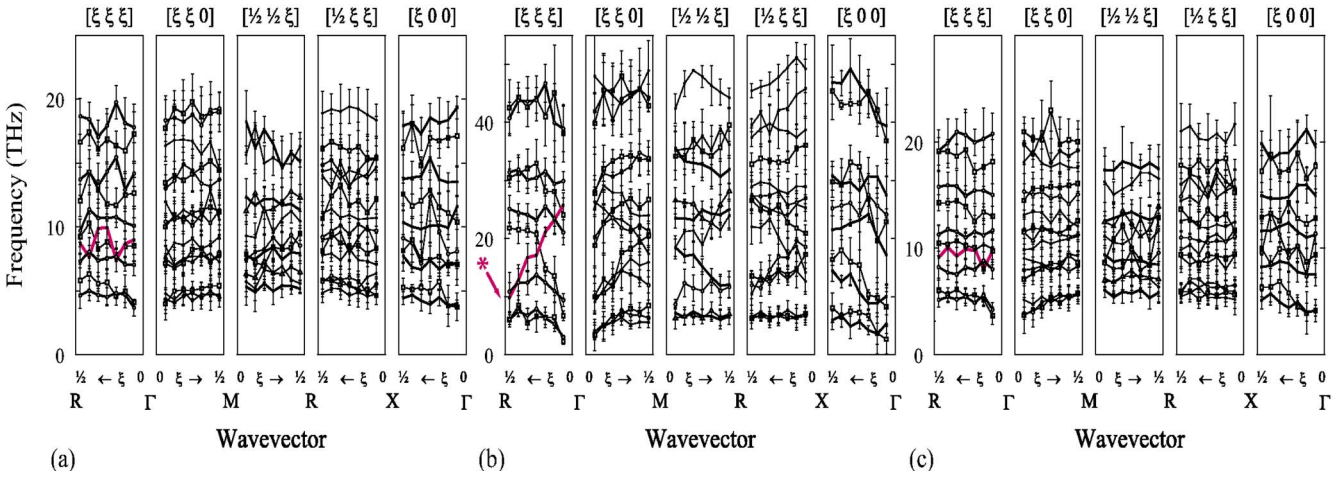

FIG. 2. (Color online) Phonon-dispersion curves calculated from equilibrium RMC ensembles containing 300 configurations, each representing a $15\times15\times15$ supercell of $SrTiO_3$. No experimental data were used in the refinement process; rather, the ensembles were refined subject to (a) no restraints or constraints, (b) bond length and bond angle restraints, and (c) DW constraints. Error bars correspond to 1σ intervals and are large in the absence of any real diffraction data to drive the refinement procedure. The $[\xi\ \xi\ \xi]\ \Lambda_{25}$ mode referred to in the text is indicated in panel (b) by an asterisk.

phonon-dispersion curves, as shown in Fig. 2(b): the set of three modes that occur at lowest frequency across the BZ correspond to translation of the Sr atoms alone, and the octahedral tilt mode can be seen to soften—as might be expected—along $[\xi\ \xi\ \xi]$ toward R.

By effectively introducing a simple potential model into the RMC refinement procedure, the restraints ensure that the configurations produced are simultaneously consistent with both the diffraction data and the potential model. If such a model were physically reasonable and applied in a manner whereby the restraints are weakly weighted with respect to the data constraints, then one might expect to arrive at rather excellent RMC configurations in this way. The restraints prevent the RMC configurations from moving toward high-entropy configurations while the data provide the finer details of the local atomic displacements within crystalline materials.

2. Distance window constraints

Irrespective of their precise form, or indeed the various numbers and types of bonds they involve, restraints of the type represented by Eq. (26) inherently impart some shape to the phonon-dispersion curves obtained. For this study, it is essential that we probe only that dynamical information present within the diffraction data themselves. Consequently, we sought to find methods of generating similarly realistic configurations using RMC without at the same time influencing the extent of dynamical information held within them.

We initially considered a "slack tether" constraint, in which atoms were tethered to their crystallographic (average) sites so that they were allowed move freely (i.e., without penalty to χ^2) within a predefined radius, but were forbidden from straying further than this distance. This constraint, like the potential restraints above, was effective at preventing the incorporation of damaged regions within the RMC configurations. However, as the atoms were tethered to some point within the configuration and not their neighboring atoms, it also prevented any correlated motion of large regions of atoms within the same configurations. The acoustic branches of the phonon dispersion no longer fell to zero frequency near the zone center as a consequence.

Eventually, we arrived at a relatively simple constraint which acts to preserve the distances between neighbors within a predefined "window" of values [referred to hereafter as the distance window (DW) constraint]. Any move proposed by the RMC algorithm that would either bring pairs of neighboring atoms too close together or separate them by too great a distance is automatically rejected. Essentially, the constraint involves the incorporation of additional terms in the calculation of χ^2_{RMC} of the form

$$\chi^2_{\mathrm{DW}} = \sum_{ij} \eta(r_{ij}), \tag{27}$$

where the δ-function-like terms $\eta(r_{ij})$ are given by

$$\eta(r_{ij}) = \begin{cases} 0, & r_{ij,\min} \leqslant r_{ij} \leqslant r_{ij,\max}, \\ \infty, & \text{otherwise}. \end{cases} \tag{28}$$

The summation typically involves those pairs of atoms (i,j) that are either nearest or next-nearest neighbors. In this way, the constraint acts to maintain a sense of connectivity throughout configurations, rather than simply removing intensity from regions of the various $g_{ij}(r)$ functions (the effect of closest-approach constraints). For each pair (i,j), the limiting values of the corresponding peak in the experimental $T(r)$ function give appropriate values of $r_{ij,\min}$ and $r_{ij,\max}$. In practice, the "window" of allowed values defined by $r_{ij,\min}$ and $r_{ij,\max}$ is often extended in order to avoid placing too strict a constraint on the configurations and to allow RMC some flexibility. DW constraints that are too restrictive can affect the peak shapes in the calculated $T(r)$ function: the tails of peaks are truncated, forcing the residual atomic density to accumulate near the cutoff values. This is readily di-

agnosed and addressed by slackening the DW constraints applied.

Configurations prepared in this way [Fig. 1(c)] lack the regions of localized damage that plague those generated without constraints, while their respective fits to data are essentially identical. Disorder in these configurations manifests itself in the form of small concerted displacements of large regions of atoms. In Fig. 1(c), the magnitude of these displacements can be seen to vary across the configuration.

The fact that χ^2_{DW} is zero-valued for any configuration with values of r_{ij} within their allowed "windows" avoids the incorporation of any bias on the phonon dispersion. An ensemble of $SrTiO_3$ configurations was generated in the same manner as that used to study the effects of the potential restraints, and the resulting set of phonon-dispersion curves calculated. Encouragingly, our results [Fig. 2(c)] illustrate that the DW constraint yields a set of featureless dispersion curves, similar in nature to those calculated from unconstrained RMC configurations. Consequently, the constraint appears to function as desired: it successfully moderates disorder in the RMC configurations while leaving the associated phonon-dispersion curves unaltered.

V. DATA COLLECTION AND REDUCTION

Having established the various theoretical and computational requirements, we turn now to describe our methods of collection and reduction of diffraction data. The quality of any dynamical information extracted from scattering data will depend on at least three experimental factors. First, we require high resolution of the pair distribution function. This is particularly relevant to the measurement of high-frequency modes, whose effect on interatomic displacements is subtle. The PDF resolution

$$\Delta r \simeq \frac{3.791}{Q_{\mathrm{max}}} \tag{29}$$

depends on the maximum observed scattering vector Q_{max}. Consequently, to resolve displacements to within a few tenths of an angstrom, we require scattering data with Q_{max} of ~ 40 Å^{-1}. This resolution might also be expected to affect the range of frequencies observable in any phonon-dispersion curves determined from the diffraction data. A second requirement is the need for the total scattering to be a good integration over all possible changes in energy, allowing both elastic and inelastic scattering events to occur. This implies that the energy of the incident neutron beam must be higher than the energy scale of the phonons in the material. High incident neutron energy also ensures that the energy integration is as close to constant Q as possible. Finally, any background scattering needs to be minimized, so that it is possible to measure scattering at high values of Q with good statistical accuracy.

The GEM instrument at ISIS is suitable for such measurements as it has (i) a large number of detector banks giving a wide coverage of Q for high-energy neutrons, (ii) a relatively low intrinsic background, (iii) relatively high resolution for measurement of Bragg peaks, and (iv) the high energy of the incident beam is sufficient to ensure that the scattering beam will include all phonon-creation processes.[12] The scattering data analyzed in this paper were collected on this instrument. However, given the advent of synchrotron sources with increasingly high-energy x-ray beams, permitting measurements to $Q_{\mathrm{max}} \sim 30$–40 Å^{-1} (albeit with weak intensities at high values of Q due to the Q-dependent x-ray form factors), we expect to see an increasing use of synchrotron x-ray beams for total scattering measurements.

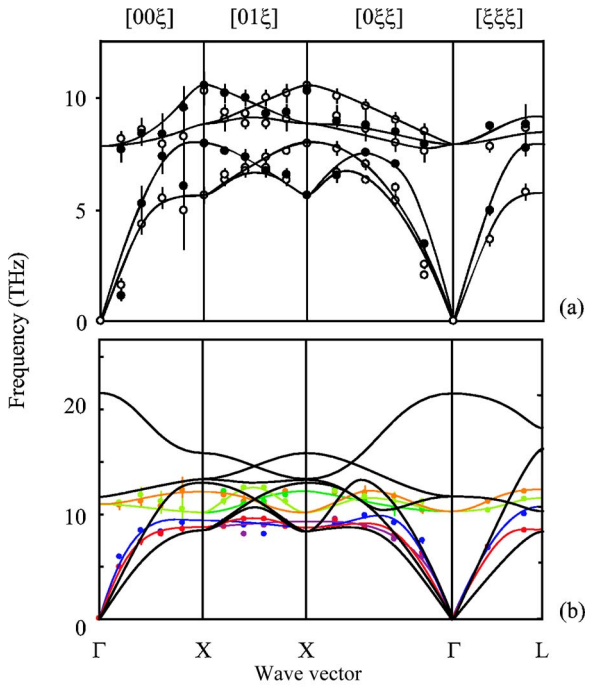

FIG. 3. (Color online) (a) MgO phonon-dispersion curves given in our initial analysis of RMC configurations derived from NPD data (Refs. 1 and 8). The lines trace equivalent modes across each symmetry direction. (b) Symmetry-adapted phonon dispersion determined as described in the text (colored data points and lines) and calculated using a standard shell lattice dynamical model from Ref. 30 (black lines).

Following their collection, the total scattering data were corrected for the effects of background scattering, absorption, multiple scattering within the sample, beam intensity variations, and the so-called Placzek correction was applied.[24] These corrected data were then converted to $S(Q)$, $T(r)$, and Bragg intensity data; all three sets were used as input for the RMC procedure in the manner described above.

VI. CASE STUDIES

We proceeded to apply our technique to two systems. The first, for which some preliminary results have recently been reported [Fig. 3(a)],[1,8] involves determination of the phonon-dispersion curves in rocksalt-structured MgO. We had chosen this system initially as its lattice dynamics, although nontrivial, are well understood.[30,31] The analysis is repeated in the present context so that, by comparison with the previously reported results, it might act as a means of assessing the merits (or otherwise) of both the symmetry-adapted approach and the DW constraint outlined above.

As a second case study, we determined the phonon-dispersion curves of $SrTiO_3$ across a range of temperatures. Its dynamical behavior, which is also well understood,[32–35] is significantly more complex than that of MgO; in particular, the material possesses two modes with strongly temperature-dependent behavior. One is at the R point of the BZ, giving rise to a displacive phase transition upon softening at 105 K. The other is at the zone center and corresponds to an incipient ferroelectric instability at low temperature. We were interested to observe whether these features were discernible in the diffraction-based phonon-dispersion curves.

A. Magnesium oxide

Neutron total scattering data were collected at room temperature on the GEM instrument at ISIS[12,13] over a range of momentum transfers $1 \leqslant Q \leqslant 42$ Å^{-1}. These data were used as input for the RMC procedure to generate an ensemble of 2000 configurations. In order to prevent the incorporation of disorder within these configurations, we employed DW constraints as discussed above, with the critical distances determined by inspection of the experimental $T(r)$ functions. The ensemble was analyzed according to the method described above along the symmetry directions $[0\ 0\ \xi]$, $[0\ 1\ \xi]$, $[0\ \xi\ \xi]$, and $[\xi\ \xi\ \xi]$ at intervals of 1/10. In contrast to the method employed in our previous report,[1] we included consideration of the crystal symmetry in the present analysis. Consequently, there is a slight improvement of the quality of our results [Fig. 3(b)]. Moreover, we were able to assign modes automatically at each wave vector, rather than relying upon tedious manual inspection of the corresponding eigenvectors.

Despite the obvious improvement in the accuracy of the phonon frequencies obtained, the same general conclusions can be drawn. First, many of the features observed in sets of phonon-dispersion curves determined using INS can be seen to occur in those reported here: the energy scale is appropriate, and the dispersion among the low-frequency modes is well reproduced. On the other hand, as we noted in our previous report,[1] the diffraction data are insensitive to any splitting of the LO and TO branches at the zone center.

We investigated the absence of any LO/TO splitting in the RMC-determined phonon-dispersion curves by generating a new ensemble of 3000 configurations with a molecular-dynamics (MD) simulation. The MD model used was a standard shell potential,[36] which is capable of reproducing LO/TO splitting at the zone center. This splitting was evident within the phonon-dispersion curves calculated from the ensemble of configurations; consequently, it is not the method of analysis itself responsible for the absence of LO/TO splitting in the RMC-derived configurations.

We subsequently generated artificial $S(Q)$, $T(r)$, and Bragg intensity data sets from the MD configurations themselves, and used these as input for the RMC procedure. A further 500 configurations were generated in this manner, using precisely the same parameters used initially to generate configurations from the experimental diffraction data. While the fits to data obtained were near perfect, the phonon-dispersion curves calculated from these configurations again lacked any LO/TO splitting at the zone center.

These results suggest there may be inherent limitations to what is possible to achieve using this approach. Even with idealized data sets (such as the MD-derived diffraction data) and data analysis capable of extracting all phonon-dispersion features—including the LO/TO splitting—it may not be possible to replicate the phonon-dispersion curves measured experimentally using spectroscopic techniques such as INS and IXS. This having been said, the low-frequency modes appear to be well preserved in the data; such modes are generally the most important, as they dominate the dynamical behavior of materials.

B. Strontium titanate

To investigate whether NPD data were sensitive to any temperature-dependent behavior of the phonon-dispersion curves in $SrTiO_3$, neutron total scattering data were collected at a range of temperatures: 105, 150, 200, 250, and 295 K. These were collected on the GEM instrument at ISIS[12,13] over a range of momentum transfers $2.2 \leqslant Q \leqslant 46$ Å^{-1}. For each temperature, the three sets were used as input for the RMC procedure to generate approximately 2000 configurations, each containing a $15 \times 15 \times 15$ array of primitive cubic unit cells. Again, in order to prevent the incorporation of disorder within these configurations, we employed DW constraints as discussed above, with the critical distances determined by inspection of the experimental $T(r)$ functions. In practice, these were the same values as those used in our evaluation of the DW constraint above, and so we were confident of their independence from the observed phonon-dispersion curves.

Each ensemble was analyzed according to the method described above along the symmetry directions $[\xi\ \xi\ \xi]$, $[\xi\ \xi\ 0]$, $[\frac{1}{2}\ \frac{1}{2}\ \xi]$, $[\frac{1}{2}\ \xi\ \xi]$, and $[\xi\ 0\ 0]$ at intervals of 1/15. Again, we included consideration of the crystal symmetry in our analysis, and so we were able to assign unambiguously the various modes at each wave vector. Our results [Figs. 4(a)–4(e)] are interesting for a number of reasons. First, there is a large degree of reproducibility in the broad dispersion features across the five temperature values. Second, the overall spread of energies is very similar to that of the earlier INS measurements [Fig. 4(f)]. Third, a significant degree of mode softening is observable both at the R point and at the zone center with decreasing temperature. Indeed, it is possible to quantify the extent to which the frequency of each mode changes over the temperature range studied. Importantly, from among all modes across the BZ, the two that exhibit the greatest rate of softening over this temperature range are—as expected—the R_{25} (octahedral tilt) mode at the R point on the zone boundary and the Γ_{15} (ferroelectric) mode at the zone center. Fourth, to a lesser extent than seen in the phonon softening discussed in the previous point, the analysis does lead to a general softening of modes across the phonon spectrum on cooling. We believe that this is an artifact of some limitations on the data quality.[37] This leads to small errors that will have the effect of adding a small component to the mean-square atomic displacements. In turn, this has a proportionally greater effect at lower temperatures, where thermal motion is

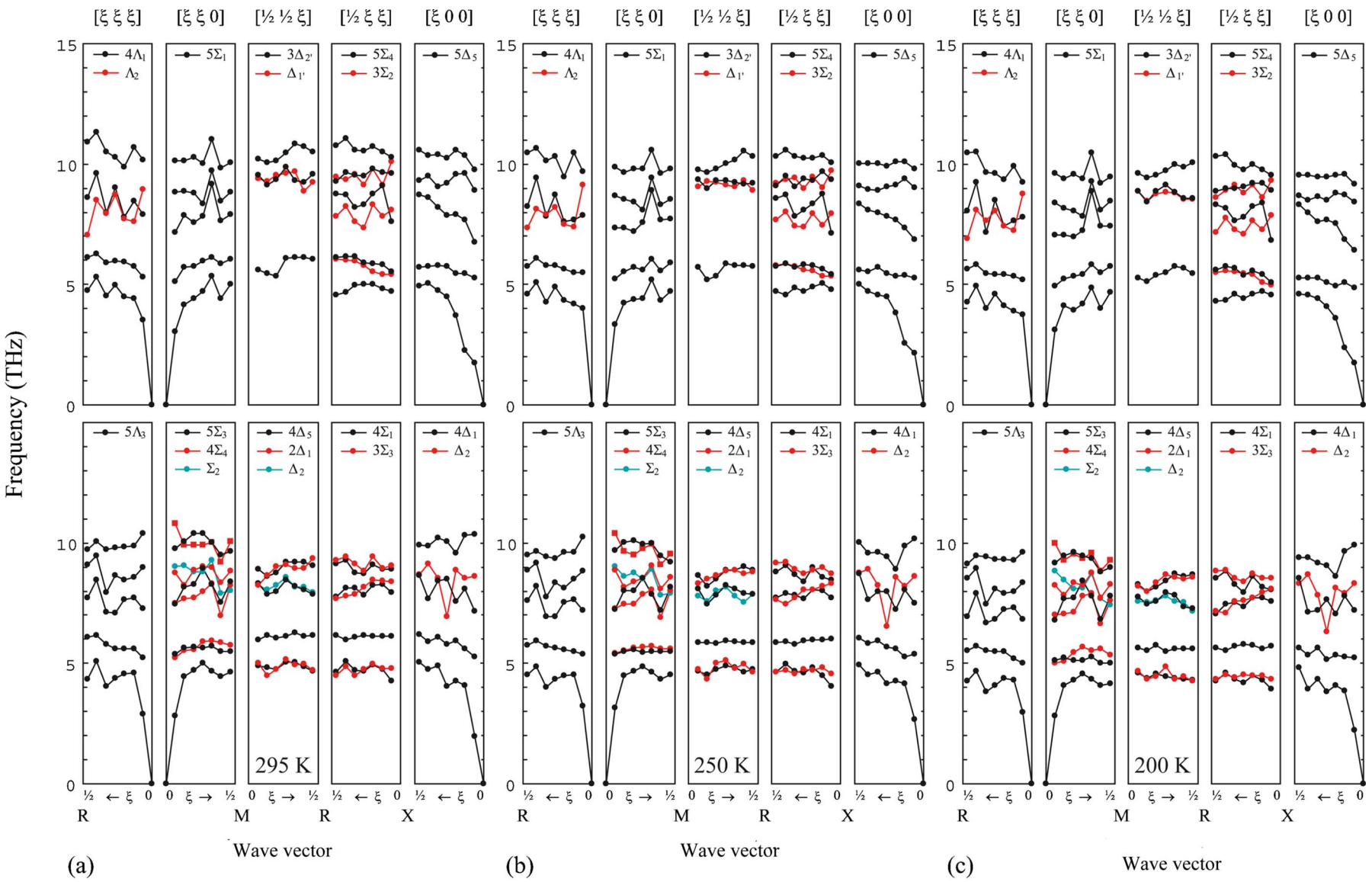

FIG. 4. (Color online) Phonon analysis of $SrTiO_3$ configurations generated using the RMC method, with NPD data collected at (a) 295 K, (b) 250 K, (c) 200 K, (d) 150 K, and (e) 105 K. The modes have been classified according to their symmetry. The softening of modes at the *R* and Γ points is evident and the relevant components of the dispersion curves have been circled; these correspond to the octahedral tilting and ferroelectric modes, respectively. (f) Phonon-dispersion curves of $SrTiO_3$ at 297 K measured by INS (Refs. 33 and 35) (filled and open circles) and from a harmonic potential model (solid lines, model 5 in Ref. 35). The high-frequency region of the plot (which extends to ~25 THz and for which no experimental data were measured) has been excluded for clarity.

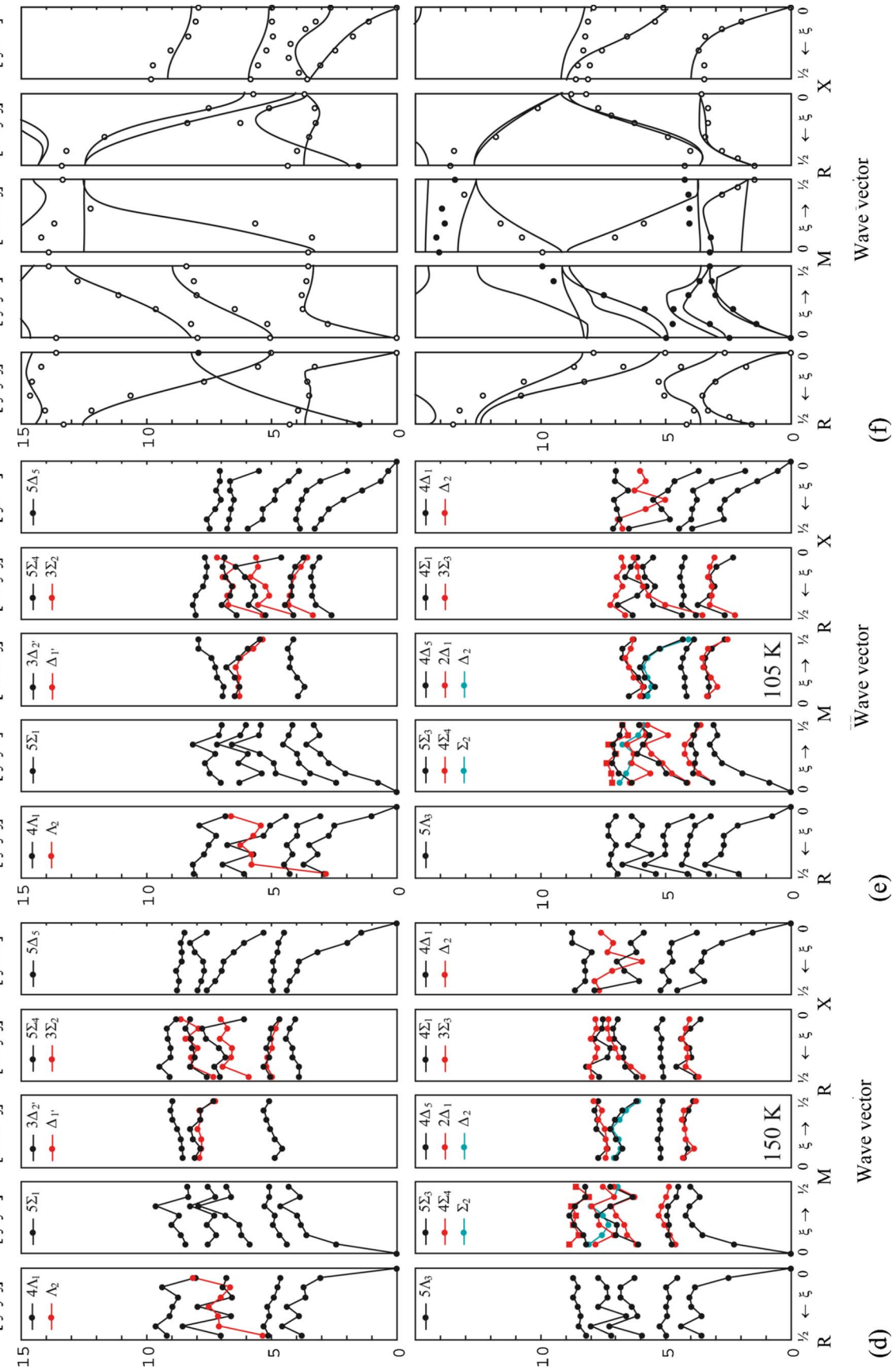

FIG. 4. (*Continued*).

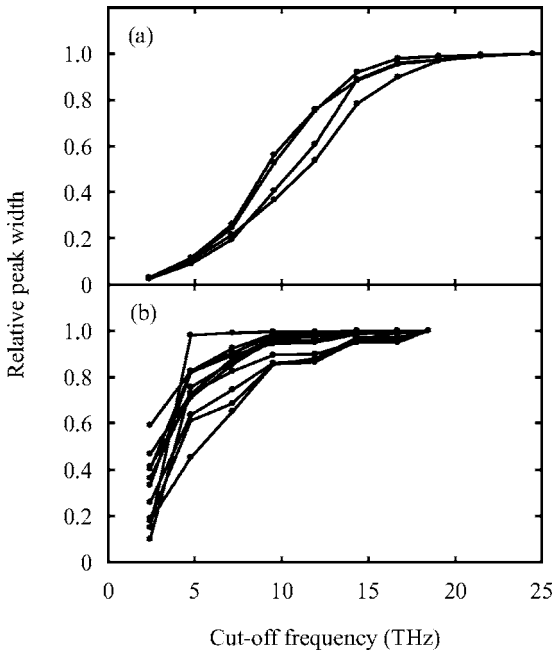

FIG. 5. Dependence of the widths of various peaks in the pair distribution function on the maximum frequency included in the sums within Eq. (1) for (a) MgO and (b) $SrTiO_3$.

lower, and the inverse relation between displacements and frequencies will lead to an underestimate of phonon frequencies at lower temperatures.

Interestingly, the details of the phonon dispersion are mostly absent from those curves measured at higher temperatures; it is only upon cooling to temperatures approaching the phase transition that features such as softening of the R_{25} and Γ_{15} modes become evident. Even at 105 K, however, it is only the low-frequency modes whose dispersion resembles that measured in INS experiments. As seen to occur for MgO, the diffraction data seem ignorant of any appreciable variation with wave vector among the high-frequency modes.

VII. THE CONTRIBUTION OF THE HIGH-FREQUENCY MODES

Because our approach has primarily run into problems in determining the behavior of the high-frequency modes, we have carried out a separate evaluation of the contributions of the high-frequency modes to the widths of the peaks in the PDF. Our approach is to compute the phonon-dispersion curves with the General Utility Lattice Program (GULP)[38] using tuned interatomic potential models, and to compute the peak widths via Eq. (1). The contribution of the higher-frequency modes can be assessed by only including certain frequency ranges in the summations in Eq. (1). Specifically, we only include contributions from zero up to a maximum frequency, ω_{max}. Figure 5 shows the results of this procedure for all the lower-r peaks in the PDF for both MgO and $SrTiO_3$. It should be noted that the complete sum in each case agrees well for both cases in comparison with experimental data. The MgO potential model used was taken from Ref. 39; the $SrTiO_3$ model was adapted from Ref. 40.

The key result from Fig. 5 is that the widths of the peaks in the PDF are relatively insensitive to a large range of frequencies above some particular value—approximately 15 THz for MgO and 10 THz for $SrTiO_3$. This result in fact is independent of the choice of temperature. However, each peak has a somewhat different sensitivity to the value of ω_{max}, which also implies that different peaks will contain independent information about the contributions of different phonons to their widths.

Based on this analysis, it is not surprising that the methods discussed in this paper have not worked as well on the higher-frequency modes as on the lower-frequency ones. Of course, this general statement is fully consistent with the fact that the contribution to the atomic displacements of any vibration of frequency ω is proportional to $k_B T/\omega$; what we have accomplished in these calculations is to quantify this point.

VIII. DISCUSSION

The two examples discussed in this paper indicate to some extent the level of dynamical information that one might or might not reasonably hope to extract from diffraction data. On the one hand, if the available information were limited to the mean-squared displacements alone (e.g., from temperature factors), we would expect the observed phonon-dispersion curves to appear as dispersionless bands across the BZ, similar to those shown in Figs. 2(a) and 2(c). The fact that we have measured relatively detailed dispersion features for both MgO and $SrTiO_3$ indicates that it is possible to access significantly more than simply mean-squared displacements. Indeed, general trends among the low-frequency modes reproduce those measured using direct spectroscopic techniques such as INS. This is important as the low-energy modes dominate dynamical behavior; consequently, knowledge of their energies and characteristic atomic displacements is invaluable in understanding their effects on a range of physical properties. On the other hand, the diffraction data appear insensitive to a number of other features of the dispersion curves. For example, the splitting of the LO and TO modes at the zone center in MgO was not observed in the measured phonon-dispersion curves. That this was true even when idealized MD-derived data sets were used suggests there are some inherent limitations to the level of dynamical information retrievable; this point has been quantified using some lattice dynamical models.

What, therefore, is the best we can hope to achieve? This question has implications for both the experimental and theoretical aspects of our analysis, and we discuss these here separately.

From an experimental viewpoint, by using NPD to measure phonon spectra we are asking much more of this type of scattering data than has been done previously. Although the data from total scattering instruments such as GEM are already of very high quality, every aspect of data collection and treatment has to be rigorously assessed and, where necessary, improved. In particular, the impact of instrumental resolution should be investigated further and a robust self-

consistency of normalization protocols between the different data sets used in the RMC refinements established. By way of an example, long-range fluctuations (such as those visible in some $SrTiO_3$ configurations [Fig. 1(c)]) may be caused by omission of low-Q data from the refinement process. These data can be difficult to normalize robustly and are often masked by the truncation ripples of the low-Q Bragg peaks in the $S(Q)$ data [truncation arising from the need to convolute $S(Q)$ with the configuration box function prior to modeling with RMC[21]]. With appropriate treatment, their inclusion may help to prepare more realistic configurations. The general message is that the better the data are, the higher the quality of the configurations—and hence the phonon-dispersion curves—will be. Consequently, we are making parallel efforts to ensure that the data collection and treatment are as reliable and as self-consistent as possible.

In terms of any theoretical limitations, it was not initially clear what level of dynamical information might be present in scattering data. In principle, refinement of the RMC configurations using Bragg scattering intensities allows us to measure the single-particle correlation functions; the use of diffuse scattering $S(Q)$ and $T(r)$ data sets gives us the pair correlation functions. One important question is whether knowledge of the first- and second-order correlation functions is sufficient to describe the phonon spectrum, or whether higher-order correlations are important. Indeed, to what extent are the possible forms of the higher-order correlation functions fixed by the first- and second-order correlation functions? This latter question has been addressed previously to some extent by Welberry and co-workers within the context of the effect of atomic ordering on diffraction patterns.[41–43] On the one hand, it was shown that two-dimensional pairwise-disordered systems (i.e., those for which the pair correlations vanish) can support many vastly different triplet correlations, each of which could be used to generate atomistic configurations that differed in their triplet correlations but would give rise to identical diffraction behavior. On the other hand, configurations with strong pair correlations were found capable of supporting only a limited range of possible triplet and higher-order correlations.[41] These results were obtained for two-dimensional systems; the extension to three dimensions may carry with it additional constraints on the relationships between pair and higher-order correlations.

In practice, most systems will inevitably lie somewhere between these two extremes, where the peaks in the PDF are neither infinitely sharp (absolute pair correlations) nor infinitely broad (zero pair correlations). In such instances, it appears that the single-particle and pair correlation functions can at best approximate the triplet and higher-order correlations, a finding suggested previously by Evans.[44] One would expect the validity of this approximation to improve with increasing strength of the single-particle and pair correlations.

The dynamical matrix $\mathbf{D}(\mathbf{k})$, however, is wholly determined by two-body terms [as described by Eqs. (16) and (18)] and by definition contains all the information required to describe the lattice dynamics. The relationship between $\mathbf{D}(\mathbf{k})$ and $\mathbf{S}(\mathbf{k})$ established in Eq. (19) gives that $\mathbf{S}(\mathbf{k})$ (the quantity extracted from the experimental data) must also contain all dynamical information, stored in the pair correlations of the atomic translations. While pair correlations alone might not necessarily give rise to a unique family of atomistic configurations (with different families determined by different triplet and higher-order correlations), this result shows that the phonons are determined uniquely by $\mathbf{S}(\mathbf{k})$. What this means is that, in principle, the diffraction data contain all necessary information to describe the lattice dynamics, and that higher-order correlation functions do not pose any problems.

This leads naturally to the important question of whether phonon-dispersion curves measured using NPD are of any practical use. Our results for MgO and $SrTiO_3$ would suggest that many important features of the phonon dispersion—the low-frequency regions, and the existence and temperature dependence of soft modes—are indeed preserved within diffraction data. With the knowledge that an attempt to extract dynamical information from such data is to some extent justified, one might find the most practical method incorporates both model-independent and model-dependent approaches; for example, the form of the high-frequency modes might be fixed by an appropriate model, allowing data-driven refinement of the (usually more important) low-frequency region. This is clearly a compromise when compared to the direct observation of mode frequencies one obtains using INS. Nevertheless, the prospect that such information might be accessible using comparatively facile experiments such as NPD is incredibly valuable when studying systems for which established spectroscopic methods are prohibitive or inappropriate.

ACKNOWLEDGMENT

We acknowledge financial support from Trinity College, Cambridge to A.L.G. and from the EPSRC (U.K.).

*Present address: ISIS Facility, Rutherford Appleton Laboratory, Chilton, Didcot, Oxfordshire OX11 0QX, United Kingdom.

†Electronic address: martin@esc.cam.ac.uk

[1] A. L. Goodwin, M. G. Tucker, M. T. Dove, and D. A. Keen, Phys. Rev. Lett. **93**, 075502 (2004).

[2] D. A. Dimitrov, D. Louca, and H. Röder, Phys. Rev. B **60**, 6204 (1999).

[3] W. Reichardt and L. Pintschovius, Phys. Rev. B **63**, 174302 (2001).

[4] M. J. Graf, I.-K. Jeong, D. L. Starr, and R. H. Heffner, Phys. Rev. B **68**, 064305 (2003).

[5] M. Schwoerer-Bohning, A. T. Macrander, and D. Arms, Phys. Rev. Lett. **80**, 5572 (1998).

[6] T. Ruf, J. Serrano, M. Cardona, P. Pavone, M. Pabst, M. Krisch,

M. D'Astuto, T. Suski, I. Grzegory, and M. Leszczynski, Phys. Rev. Lett. **86**, 906 (2001).
[7] I.-K. Jeong, R. H. Heffner, M. J. Graf, and S. J. L. Billinge, Phys. Rev. B **67**, 104301 (2003).
[8] A. L. Goodwin, M. G. Tucker, M. T. Dove, and D. A. Keen, Phys. Rev. Lett. **95**, 119901(E) (2005).
[9] R. Kaplow, B. L. Averbach, and S. L. Strong, J. Phys. Chem. Solids **25**, 1195 (1964).
[10] R. Kaplow, S. L. Strong, and B. L. Averbach, Phys. Rev. **138**, A1336 (1965).
[11] J. S. Chung and M. F. Thorpe, Phys. Rev. B **55**, 1545 (1997).
[12] W. G. Williams, R. M. Ibberson, P. Day, and J. E. Enderby, Physica B **241**, 234 (1998).
[13] A. C. Hannon, The General Materials Diffractometer, http://www.isis.rl.ac.uk/disordered/gem/gem_home.htm
[14] M. T. Dove and R. M. Lynden-Bell, Philos. Mag. B **54**, 443 (1986).
[15] M. T. Dove, *Introduction to Lattice Dynamics* (Cambridge University Press, Cambridge, 1993).
[16] A. A. Maradudin and S. H. Vosko, Rev. Mod. Phys. **40**, 1 (1968).
[17] J. L. Warren, Rev. Mod. Phys. **40**, 38 (1968).
[18] In practice, the restriction is in terms of action by the Fourier transform of these symmetry operations rather than the operations themselves; the distinction is not important to the current discussion.
[19] T. G. Worlton and J. L. Warren, Comput. Phys. Commun. **3**, 88 (1972).
[20] M. G. Tucker, D. A. Keen, and M. T. Dove, Miner. Mag. **65**, 489 (2001).
[21] M. G. Tucker, M. T. Dove, and D. A. Keen, J. Appl. Crystallogr. **34**, 630 (2001).
[22] D. A. Keen, M. G. Tucker, and M. T. Dove, J. Phys.: Condens. Matter **17**, S15 (2005).
[23] D. A. Keen, J. Appl. Crystallogr. **34**, 172 (2001).
[24] M. T. Dove, M. G. Tucker, and D. A. Keen, Eur. J. Mineral. **14**, 331 (2002).
[25] D. A. Keen, Phase Transitions **61**, 109 (1997).
[26] D. A. Keen, *Local Structure from Diffraction*, edited by M. F. Thorpe and S. J. L. Billinge (Plenum, New York, 1998).
[27] M. G. Tucker, M. P. Squires, M. T. Dove, and D. A. Keen, J. Phys.: Condens. Matter **13**, 403 (2001).
[28] Q. Hui, M. G. Tucker, M. T. Dove, S. A. Wells, and D. A. Keen, J. Phys.: Condens. Matter **17**, S111 (2005).
[29] The values of $\bar{\theta}$ and σ_{angles} are three-body parameters and so do not appear directly in the PDF; however, they can be estimated by consideration of the three associated pair distributions. Alternatively, knowledge of the structural chemistry of a species—bond angles of 109.5° in tetrahedral moieties, for example—can be used to provide appropriate values.
[30] M. J. L. Sangster, G. Peckham, and D. H. Saunderson, J. Phys. C **3**, 1026 (1970).
[31] G. Peckham, Proc. Phys. Soc. London **90**, 657 (1967).
[32] R. A. Cowley, Phys. Rev. Lett. **9**, 159 (1962).
[33] R. A. Cowley, Phys. Rev. **134**, A981 (1964).
[34] G. Shirane and M. Yamada, Phys. Rev. **177**, 858 (1969).
[35] W. G. Stirling, J. Phys. C **5**, 2711 (1972).
[36] D. Fincham, W. C. Mackrodt, and P. J. Mitchell, J. Phys.: Condens. Matter **6**, 393 (1994).
[37] The problem is that there is an inconsistency in how the position of the Bragg peak is defined in the data reduction method for the Bragg diffraction data and total scattering data. This is concerned with setting the calibration of the Q scale. For separate analysis of Bragg diffraction data by Rietveld analysis and of total scattering by PDF analysis alone, this has no practical consequences, but when analyzing the two data sets together it does cause problems when including instrument resolution for all data sets which we are not yet able to completely solve. Ongoing work is being carried out in this regard.
[38] J. D. Gale and A. L. Rohl, Mol. Simul. **29**, 291 (2003).
[39] P. S. Baram and S. C. Parker, Philos. Mag. B **73**, 49 (1996).
[40] M. J. Akhtar, Z.-U.-N. Akhtar, R. A. Jackson, and C. R. A. Catlow, J. Am. Ceram. Soc. **78**, 421 (1995).
[41] T. R. Welberry, Rep. Prog. Phys. **48**, 1543 (1985).
[42] T. R. Welberry and R. L. Withers, J. Appl. Crystallogr. **24**, 18 (1991).
[43] T. R. Welberry and B. D. Butler, J. Appl. Crystallogr. **27**, 205 (1994).
[44] R. Evans, Mol. Simul. **4**, 409 (1990).